2.4 Radiation Damage of Insertion Devices at PETRA III – A Perspective View from Optics and Tracking Studies

M. Bieler, J. Keil, G. Kube, G.K. Sahoo, M. Tischer, R. Wanzenberg
Deutsches Elektronen Synchrotron, Notkestraße 85, Hamburg, Germany.
Mail to: gajendra.kumar.sahoo@desy.de

A. Kling
Institute of Dual Cooperative Studies, Osnabrück University of Applied Sciences,
Kaiserstraße 10b, Lingen, Germany.
Mail to: A.Kling@hs-osnabrueck.de

2.4.1 Introduction

PETRA III [1, 2] is a 3rd generation synchrotron light source operating with electrons at a beam energy of 6 GeV. PETRA was originally built in 1976 as an electron - positron collider and was used as a preaccelerator for the HERA lepton hadron collider ring from 1988 to 2007 (PETRA II). After the end of the HERA collider physics program PETRA II was converted into a dedicated synchrotron radiation facility (PETRA III). It has a large circumference of 2304 m which is considerably larger than any existing light source. The machine consists of arcs and several straight sections. The so-called long straights which have a length of 108 m are located in the North, East, South and West. In between two long straights are two arcs and short straight sections with a length of 64.8 m. The magnetic structure of the arcs is a simple FODO lattice. The part that extends from the middle of one long straight to the middle of the adjacent short straight is the basic building block of the machine. Since this section is just one eighths of the machine it is called an octant. The magnetic arrangement of one octant is mirror reflected at the middle of the short straight. Electrons are injected in the South-East (SE) and travel clockwise around the machine. The octant extending from North-East to East was modified breaking the fourfold symmetry and is called as new octant (built in the building Max von Laue Hall). It consists of eight double bend achromat cells (DBA). The DBA-cells provide space for one 5 m or two 2 m long insertion devices (ID). The two 2 m IDs are inclined towards each other by 5 mrad. This scheme allows operating two independently tunable undulators in a single straight section with beam paths sufficiently separated for individual beam line optics. In the North-East a ninth straight section is suitable for the installation of an insertion device up to a length of 10 to 20 m. The horizontal beam emittance is 1 nm rad while a coupling of 1% amounts to a vertical emittance of 10 pm rad. The machine is dedicated to users at 14 beam lines with 30 end-stations. Parts of the storage ring [3] have recently been reconstructed to accommodate 10 new beamlines and additionally a super luminescence near UV beamline providing bending magnet radiation. PETRA III operates with several filling modes, such as 40, 60, 240, 480 and 960 equally spaced bunches with a total beam current of 100 mA.

The IDs and other accelerator components are expected to experience extreme radiation in synchrotron light sources especially where higher beam energies, beam currents and smaller gaps are in place. It is worth to mention that, permanent magnets operating under conditions of high radiation are especially susceptible to demagnetization [4] caused by direct and scattered radiation induced by electrons, positrons, high-energy photons and neutrons. Serious demagnetization has been observed in some of the operating light sources such as ESRF, where insertion devices experienced field losses of as much as 8% [5] and at the APS [6]. Here we report on partial demagnetization profiles, which are not linear along the device [7, 8, 9]. Similar loss patterns are also clearly seen in tracking results. To protect the IDs additional collimators have been recently installed at PETRA III.

2.4.2 Observation of Radiation Damage of Insertion Devices

Radiation damage of machine hardware, electronics and magnet structures have been observed for some time in PETRA III. First signs of radiation damage were observed in the damping wiggler sections and in the form of rust on undulators as shown in Figure 1. On the other hand, performance losses have been observed at several beam lines. The gaps operated at some beam lines have to be decreased or tapers introduced over time and distortions of higher harmonics have been observed, as depicted in Figures 2 and 3. Beam lines suffering from performance losses are in most cases not affected by the appearance of rust on their IDs, as can be seen in Figure 1. PU08 (PETRA Undulator 08) shows significant loss in performance but essentially no sign of rust, while PU09 (located in the same canted straight section) shows essentially no sign of field deterioration of the insertion device but significant signs of rust. In the following, we will focus on the aspect of performance losses. Different measures have been taken to mitigate the rust problem (i.e., better control of tunnel humidity, improved orbit control in upstream dipoles, etc.).

Inspection of the magnetic structures and in-situ magnetic measurements revealed a partial demagnetization of devices exhibiting performance losses. Some results of these measurements are summarized in Figures 4, 5 and 6. Devices located upstream in canted straight sections as PU02 and PU08 are damaged at the upstream end of the magnet structure while the downstream located device PU03 is damaged at the downstream end (see Figures 4 and 5). The measured decrease of the peak field is attributed to radiation damage and is most likely caused by particle losses.

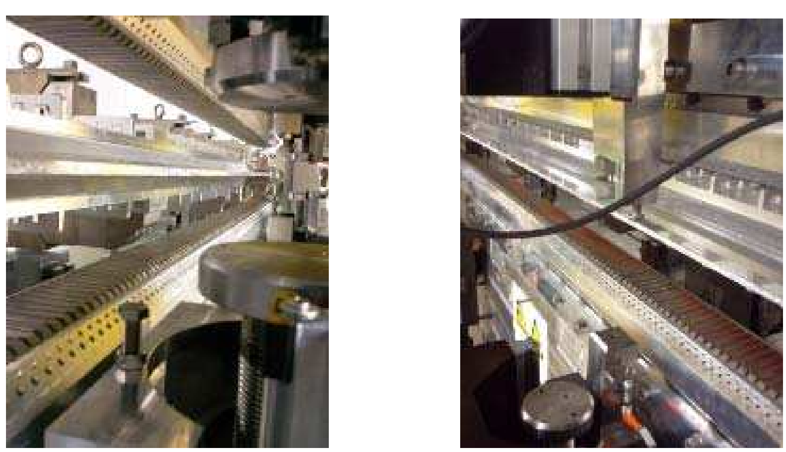

Figure 1: The magnetic structure of undulators PU08 (left) and PU09 (right). On PU09 significant signs of rust are clearly visible.

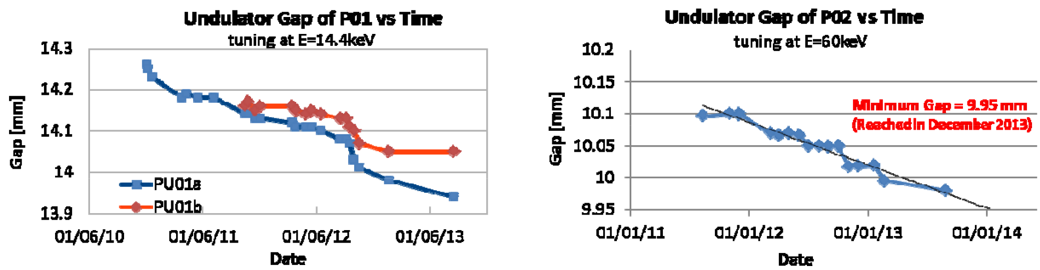

Figure 2: Gap vs. operation time of undulators PU01 and PU02. Both undulators observe performance losses.

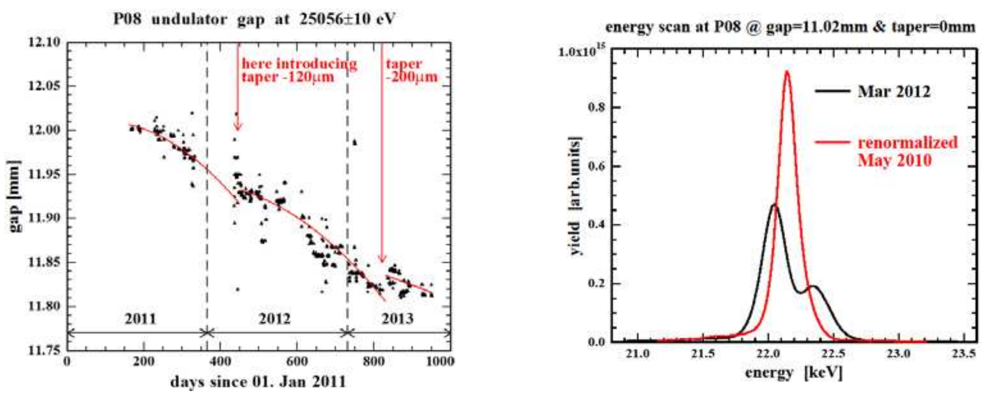

Figure 3: Left: Gap vs. operation time of undulator PU08. The introduction of tapers partially compensates the performance loss by accounting for the linear part of the demagnetization. Right : Distortion of the 5th harmonic at PU08 due to radiation damage of the ID.

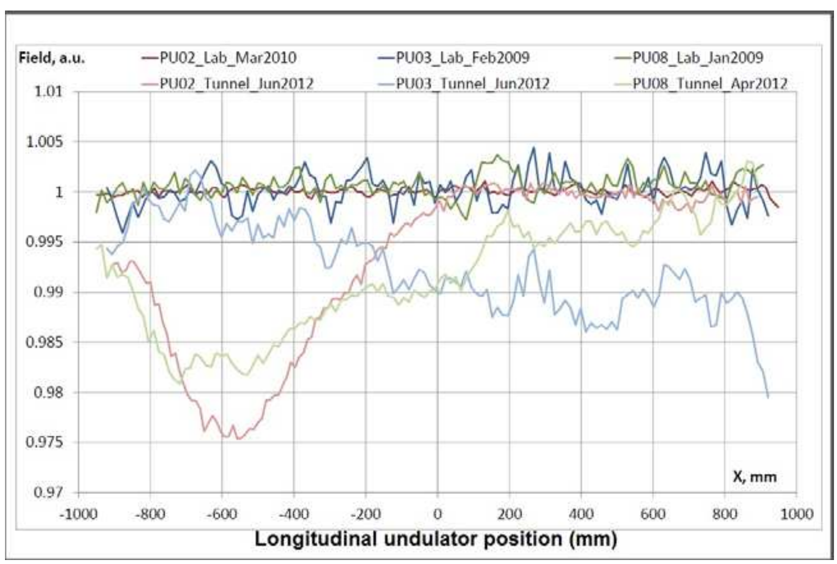

Figure 4: In-situ magnetic measurements reveal a loss of up to 2.5% in peak field at certain insertion devices. Devices located upstream in canted straight section as PU02 and PU08 are damaged at the upstream end of the magnet structure while the downstream located device PU03 is damaged at the downstream end.

The rationale behind this hypothesis is that in particular PU01 is affected. PU01 is located at the center of an almost 70 meters long straight section in north east. The upstream and downstream dipoles are comparatively far away. Moreover, the upstream dipole is a weak 5.3 meters long standard old octant dipole. The background of synchrotron radiation is most likely low at PU01. However, PU01 has the first low gap chamber at the entrance to the experimental hall. Particles with large vertical amplitude are likely to be intercepted at this point. The same refers to PU02 where the vertical aperture is even smaller (7 mm at PU02 vs. 10.5 mm at PU01). PU08 is most likely affected because it was the first beam line to be commissioned in early stages of PETRA III operation and probably has accumulated radiation doses, possible also in less controlled machine states.

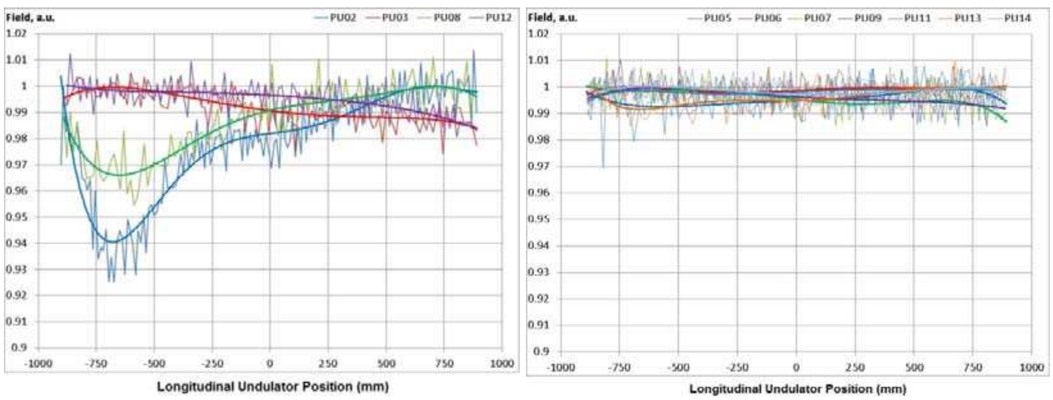

Figure 5: Measured longitudinal peak field variation of the 2 m devices installed in PETRA III. The left picture shows devices with signs of damage while the right picture shows devices with essentially no sign of demagnetization.

A similar situation as for the 2 m devices located in canted straight sections is observed for the 5 m long devices installed in PETRA III (Figure 6). In sector 1 the 5m undulators PU01a and PU01b are installed side by side. The upstream device PU01a is strongly damaged at the upstream end. The downstream located device PU01b shows no sign of demagnetization. This is somewhat surprising because anticipating results from beam loss monitor (BLM) measurements the downstream end of sector 1, where PU01b is installed, shows high loss rates as measured by the BLMs. The undulators PU01a and PU01b are usually operated together, nevertheless these undulators seem not been exposed to beam losses in a comparable way. Data taken for the 5 m device PU10 also confirm the damage pattern observed at the 2 m devices installed in the canted straight sections. The undulator is installed in a standard (not canted) straight section. PU10 shows signs of demagnetization at the entrance and the exit of the device. Moreover, a comparison of data taken in 2012 and 2013 shows that in spite of the decreasing total dose measured with thermo-luminescent dosimeters (TLDs) the damage seems to continue unabatedly.

In the Figure 6, data plotted in green show the situation at PU10 which is a 5m device located in a standard straight section (not canted). The characteristics of the magnetic damage follow the pattern of the 2m devices in the canted straights. The damage occurs at the entrance and the exit of the straight section and the damage of the upstream part are more severe than the damage of the downstream part. The figure on the right compares measurements of PU01a from 2012 and 2013 to the measurement of PU01b. From the shown data it is clear that the magnetic deterioration continues, although the total radiation dose measured by TLDs is reduced from year to year.

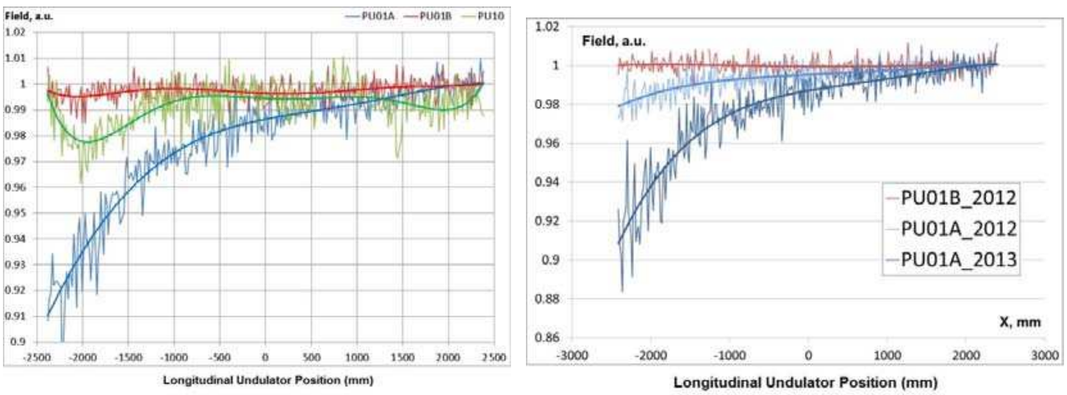

Figure 6: Left: Previously measured 5 m devices installed in PETRA III. PU01a and PU01b are located in sector 1 and both serve beamline P01. The upstream device PU01a shows strong signs of demagnetization, while the downstream device PU01b is not affected.

In summary, radiation damage of insertion devices is observed at several places of the PETRA III undulator sections. It follows a general pattern that devices located at the entrance of a straight section are damaged at the entrance end while undulators installed at the exit of a straight section show signs of demagnetization at the exit end. This seems to indicate that particle losses occur in the vertical plane at locations where the beta functions become large while the physical aperture limits are still very small.

2.4.3 Diagnostic Tools

In the following section, a number of diagnostic tools available for the detection of radiation in PETRA III are described. Some of them were originally not intended to detect sources of radiation damage.

2.4.3.1 TLDs

The insertion devices group at the photon science department regularly installs thermo luminescent dosimeters (TLDs) and evaluates the measured radiation doses.

2.4.3.1 Beam Loss Monitors

Originally, no beam loss monitors (BLMs) were foreseen in PETRA III. Already at an early stage of the commissioning phase, a BLM system has been installed which was previously used in the HERA electron accelerator. The monitors as shown in Figure 7 consist of two reversely biased PIN-photodiodes, mounted face-to-face with a 300 µm thin copper layer in between. Charged particles which cross both diodes produce coincidence signals with a high efficiency, while the efficiency of coincident signals from photons from synchrotron radiation is very small. The copper layer additionally helps to reduce spurious coincidence signals from Photo- or Compton-electrons, generated by synchrotron radiation in one diode, which may reach the other one. While the coincidence mode is mainly sensitive on charged particle losses, it can remotely be switched off such that it is also possible to measure the count rate of a single diode which is dominated by synchrotron radiation background. With this system it is possible to count beam losses up to the maximum frequency of 10.4 MHz. More details can be found e.g. in Ref. [17].

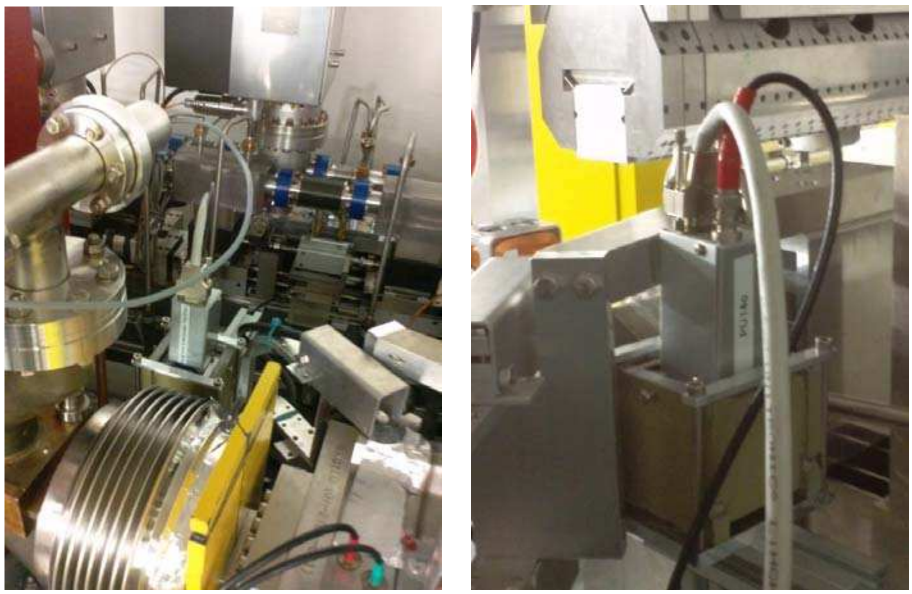

Figure 7: Beam loss monitors in PETRA III. Each section is now equipped with an upstream and a downstream BLM.

2.4.3.1 Cherenkov Fibers

The BLM system is a counting system and therefore not sensitive on the amplitude of the particle losses. Therefore, as a test, a “Cherenkov fiber”-based loss monitor system has been temporarily installed in sector 1 and sector 2, along the most affected insertion devices PU01(A, B), PU02 and PU03 as shown in Figure 8. This system is originally designed to monitor beam losses in the undulator section of the VUV-FEL FLASH [18] and was temporarily installed at PETRA III for test experiments.

Figure 8: Temporarily installed Cherenkov fibers in sections 1 and 2 along beamlines P01, P02 and P03.

2.4.3.1 PANDORAS

A number of radiation detection devices called PANDORA (**P**hoton **A**nd **N**eutron **D**ose **R**ate meter for **A**ccelerators) [20] sensitive to different types of radiation are installed outside the tunnel for radiation protection. Several measurements using those types of devices have been performed to cross-check results obtained by other means of detection.

2.4.4 Measurements

The diagnostics tools are used to detect the exposure of the insertion devises to radiation. The results from the TLD measurements, the beam loss monitors and first test of the Cherenkov fibers are reported.

2.4.4.1 TLD Measurements

Every insertion device installed in PETRA III (including the damping wigglers) is monitored with respect to its exposure to radiation using TLDs. From the first day of installation of the devices TLDs are directly mounted to the devices (upstream and downstream) and regularly replaced and evaluated. The integrated dose accumulated of every device is showed in Figure 9.

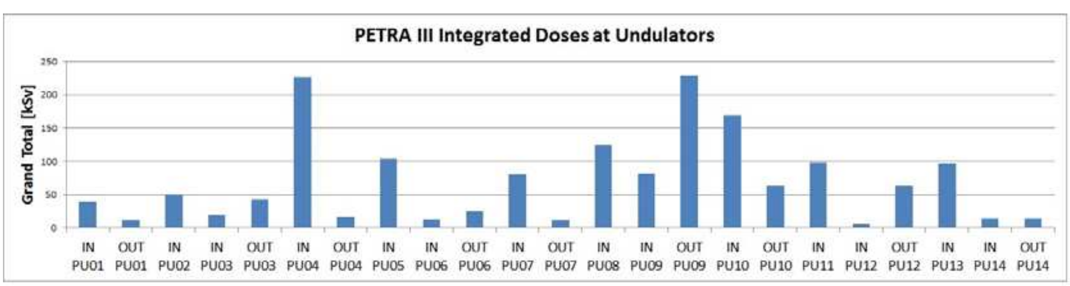

Figure 9: Integrated radiation dose accumulated at every insertion device from the first day of its installation as measured by TLDs.

The integrated dose as measured by the TLDs varies strongly from device to device and does not show any regular pattern. Even from run period to run period the accumulated dose may vary over orders of magnitude as can be seen in Figure 10, where the integrated dose for the first four run periods of 2013 is shown. In Figure 11, the yearly integrated dose accumulated at all TLDs from 2011 to 2013 normalized to the integrated current stored is shown. The integrated dose has been reduced by almost a factor of 3. Since TLDs are sensitive to particle losses and synchrotron radiation it is hard to distinguish relevant from 'harmless' parts of the measured radiation. Moreover, it is known from beam loss monitor measurements that the synchrotron radiation background strongly varies with closed orbit distortions in upstream dipoles. As stated earlier, the appearance of rust on some of the devices is attributed to unfavorable steering in upstream dipoles. Although a (long term) damage of insertion devices due to this mechanism is not ruled out the observed demagnetization effects are most likely not caused by synchrotron radiation.

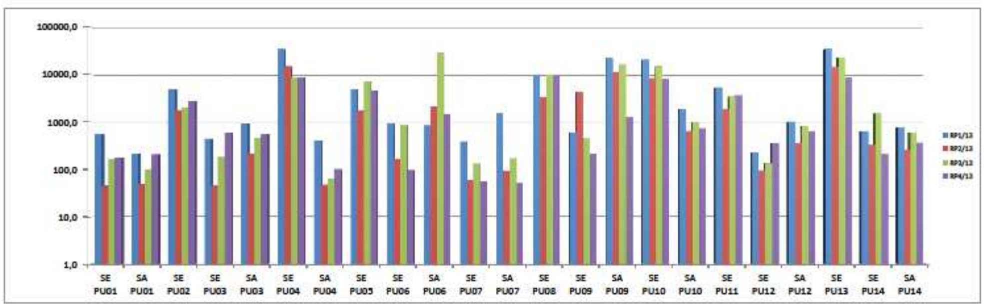

Figure 10: TLD measurement of the integrated radiation dose for the first four run periods in 2013.

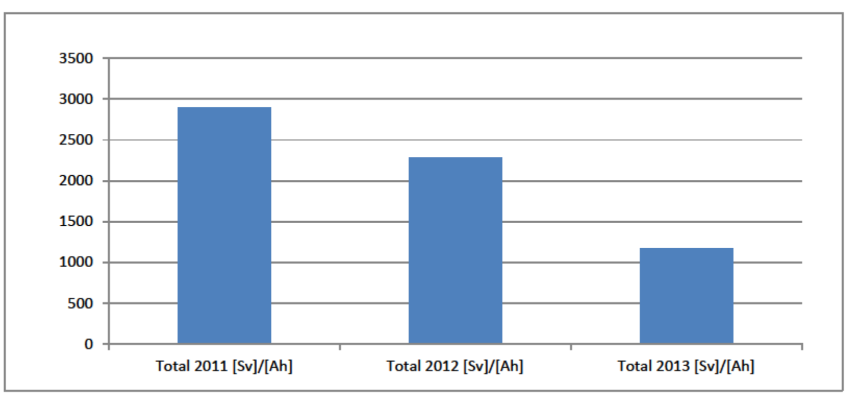

Figure 11: Yearly integrated dose accumulated at all TLDs from 2011 to 2013 normalized to the integrated current stored. The integrated dose has been reduced by almost a factor of 3.

2.4.4.2 Beam Loss Monitor Studies

In order to obtain a clearer picture of the particle losses causing radiation damage, studies have been performed using the beam loss monitors installed at the entrance and the exit of each straight section. The studies compare BLM signals recorded in the 960 bunch mode (standard continuous mode) and signals collected in the 40 bunch mode (standard timing mode). In order to quantify the effect of the collimators on different loss modes, the set points of the collimators are varied during the measurements from the nominal value applied during user operation to fully open. The measurements have been performed in Top-Up operation in order to quantify the injection losses. The current and lifetime during the measurements are depicted in Figure 12. A comparison of the integrated count rates during injection (see Figure 13, 14) and standard stored current operation (see Figure 15) shows that in both cases the integrated count rate is high in the first part of the undulator section of PETRA III. In particular, BLM 1 corresponds to the entrance of PU01a and BLM 2 corresponding to the exit of PU01b show high count numbers.

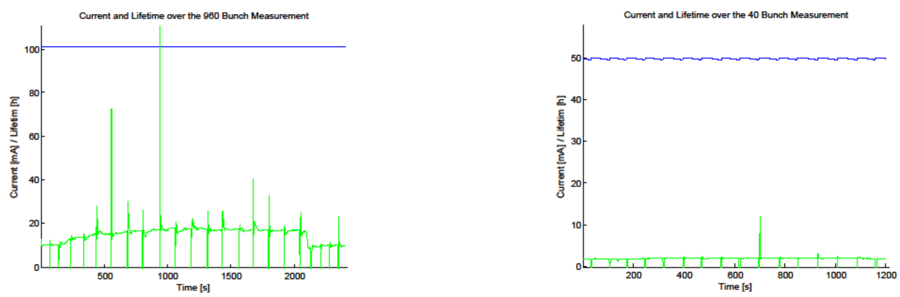

Figure 12: Current and lifetime during the beam loss monitor studies. The left picture shows the measurement using the 960 bunch mode with 100 mA; while the right picture shows the 40 bunch mode measurement with 50 mA.

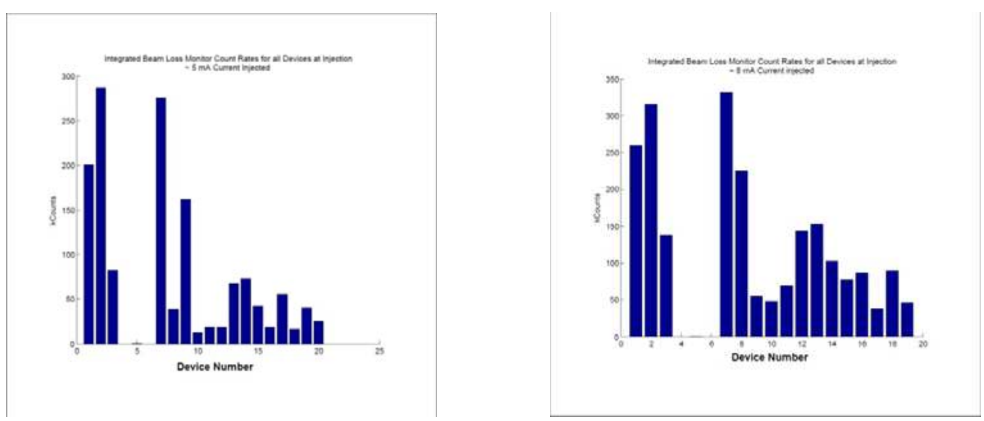

Figure 13: Integrated count rates measured during injection in the 960 (left) and 40 (right) bunch mode. The total injected current is approximately 5mA (in ~25 injections) in the 960 bunch mode and around 8 mA (in ~16 injections) in the 40 bunch mode. Data from the BLMs 4 to 6 were not available due to technical reasons.

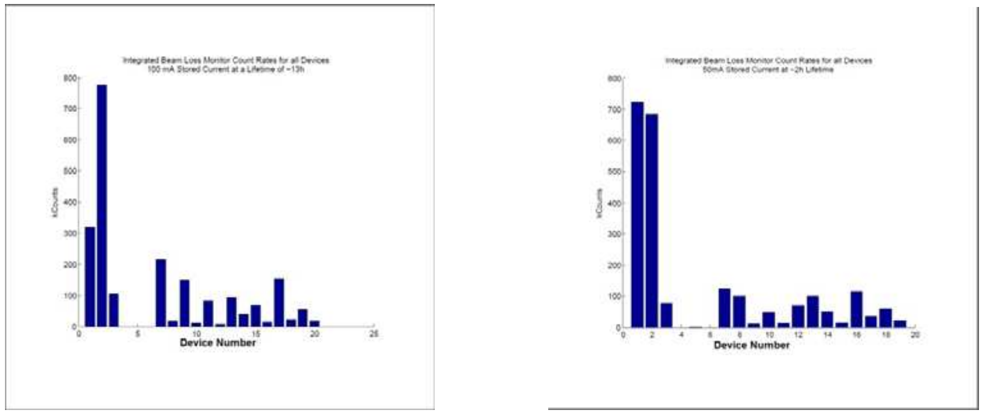

Figure 14: Integrated count rates measured during stored current operation in the 960 (left) bunch mode at 100 mA and a life time of ~10 to 15 hours and 40 (right) bunch mode at 50 mA and a lifetime of ~2 hours.

During injection the integrated rates can be significant also at other insertion devices. The integrated rates during normal stored beam operation are strongly peaked at BLM 1 and BLM 2 located in sector 1 housing beamline P01. Interestingly, the highest rates are measured at the downstream end of PU01b. However, that device does not show any signal of radiation damage!

While the measured count rates during injection are directly comparable in both operation modes, the count rates during stored current operation have to be scaled for the 40 bunch mode. During timing mode user operation usually a current of 80 mA (or even 100 mA in some run periods) is stored in 40 bunches. In the 40 bunch mode the lifetime and therefore the loss rate is dominated by Touschek scattering and scales approximately linear with the stored current. Moreover the total loss rate is proportional to the stored current. Therefore the integrated count rate at the BLMs has to be scaled by at least a factor of 3-4 to be in correspondence with standard user operation in timing mode. The total time of measurement is two times longer in the 960 bunch case, which has to be compensated by an additional factor of 2 in the 40 bunch case.

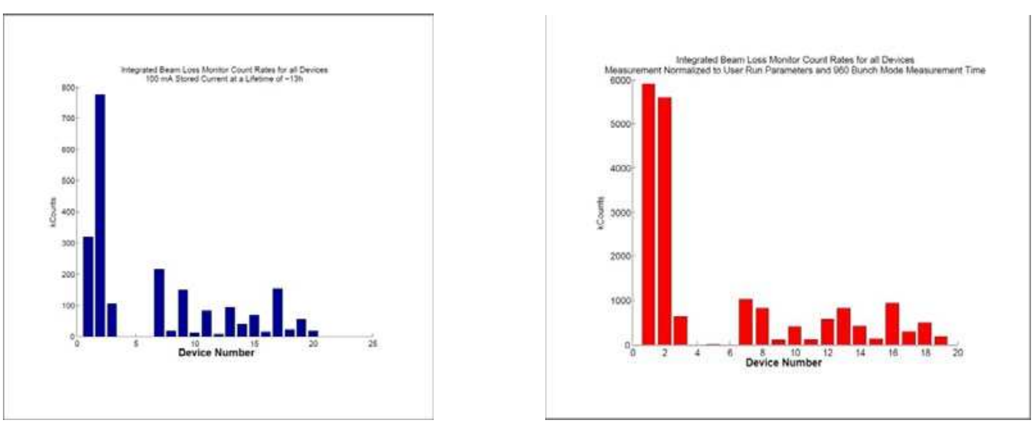

Figure 15: Integrated count rates measured during stored current operation in the 960 (left) bunch mode at 100 mA and a life time of ~10 to 15 hours and 40 bunch mode at 50 mA and a lifetime of ~2 hours taking into account the scaling to standard user operation parameters and normalized.

2.4.4.3 960 Bunch Mode

Looking at the dependency on the collimator settings for particular devices in the 960 bunch mode the effect of the collimators is clearly visible although they are located almost exactly half the ring upstream in the short straight section south-west, see Figures 16 and 17. However, while in the case of injection losses the count rates can be reduced by almost two orders of magnitude, the count rate during normal stored current operation is reduced by a factor of 3-5. Moreover, the injection losses could be further reduced by closing the collimators beyond their nominal set points, of course on the cost of reducing the injection efficiency severely, which renders this step questionable. Losses in stable beam operation are hardly further reduced already several millimeters before the collimators reach their nominal set points.

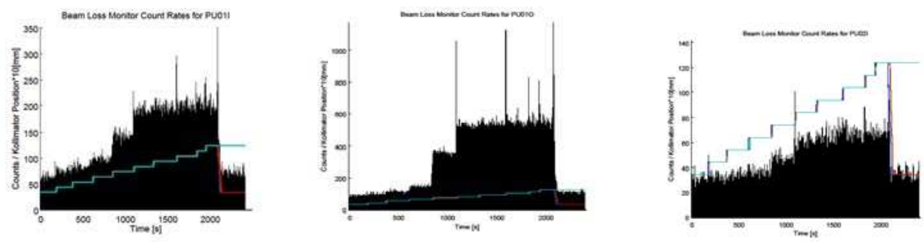

Figure 16: Count rates measured at BLM 1 (PU01a), BLM 2 (PU01b) and BLM 3 (PU02) during stable beam operation with 100 mA in 960 bunches. When opening the collimators stepwise the count rates increase by a factor of 3-5.

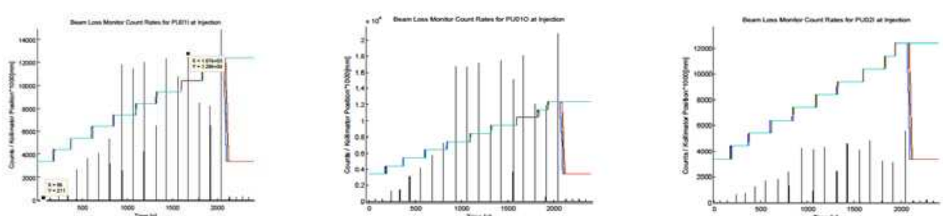

Figure 17: Count rates measured at BLM 1 (PU01a), BLM 2 (PU01b) and BLM 3 (PU02) during injection at 100 mA in 960 bunches. At every injection approximately 0.2mA was injected. When opening the collimators step wise the count rates increase by almost 2 orders of magnitude.

A comparison of the integrated losses during injection and during stable beam operation over time at 100 mA in 960 bunches shows that at (almost) all BLMs the accumulated counts during stable beam operation outbalance the counts accumulated during injection. This statement has to be taken with care since the BLMs do not provide amplitude information of the losses. This means in turn that the true losses during injection could be larger by some (unknown) factor and the measurement only provides a kind of lower limit.

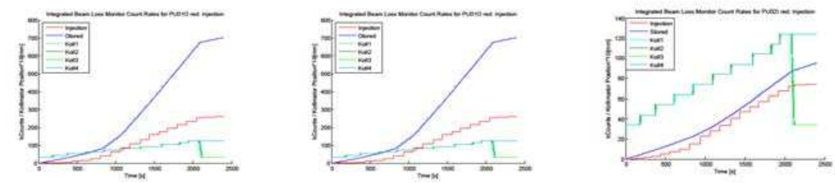

Figure 18: Comparison of the integrated losses during injection and during stable beam operation over time at 100 mA in 960 bunches. At all shown BLMs the accumulated counts during stable beam operation outbalance the counts accumulated during injection.

2.4.4.4 40 Bunch Mode

In the timing mode the situation is essentially the same as in the 960 bunch mode with the only important difference that the count rates are considerably higher due to low lifetime by Touschek dominated scattering. The count rates during stable beam operation have still to be scaled to standard user run parameters which amounts to a factor of ~4.

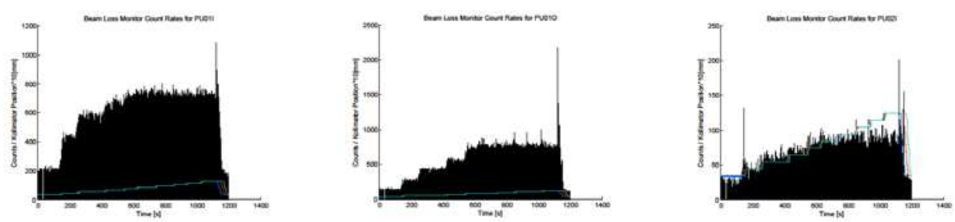

Figure 19: Count rates measured at BLM 1 (PU01a), BLM 2 (PU01b) and BLM 3 (PU02) during stable beam operation with 50 mA in 40 bunches. When opening the collimators stepwise the count rates increase by a factor of 3-5.

Interestingly, the stable beam count rates are significantly reduced also at collimator set points close to nominal values. This could be an indication that the dominating loss mechanism is different in the 960 and 40 bunch mode.

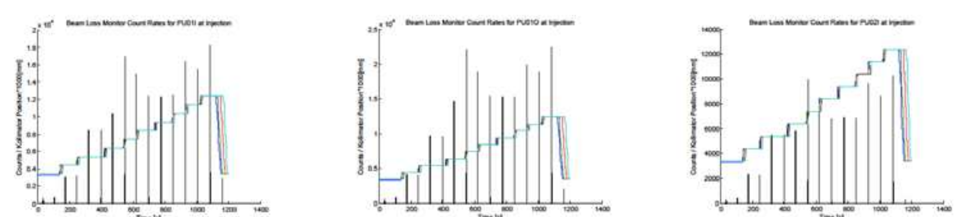

Figure 20: Count rates measured at BLM 1 (PU01a), BLM 2 (PU01b) and BLM 3 (PU02) during injection at 50 mA in 40 bunches. At every injection approximately 0.5 A are injected. When opening the collimators stepwise the count rates increase by almost 2 orders of magnitude.

A comparison of the integrated losses during injection and during stable beam operation over time at 50 mA in 40 bunches shows the same characteristics as in the 960 bunch mode. At (almost) all BLMs the accumulated counts during stable beam operation outbalance the counts accumulated during injection. This situation becomes even more clear when one takes into account that the stable beam losses have to be scaled by at least a factor of 3 to 4 while the injection losses not. However, the weight factor of the injection losses is still an unknown (see above).

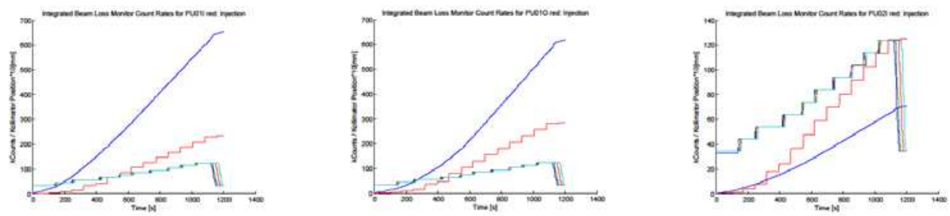

Figure 21: Comparison of the integrated losses during injection and during stable beam operation over time at 50mA in 40 bunches. At all BLMs shown the accumulated counts during stable beam operation outbalance the counts accumulated during injection. This becomes even more prominent if the scaling to standard user operation parameters is taken into account (see text).

2.4.4.5 Comparison with BLM 14 (PU09O : Exit end of PU09)

It is interesting to compare the results for devices exhibiting signs of damage presented above with measured data at BLM 14 corresponding to the downstream end of PU09. P09 was also one of the first beam lines to be commissioned so that one could expect sign of damage also from early periods with less controlled beam operation. However, this is not the case. The corresponding measurements are shown in Figures 22 and 23.

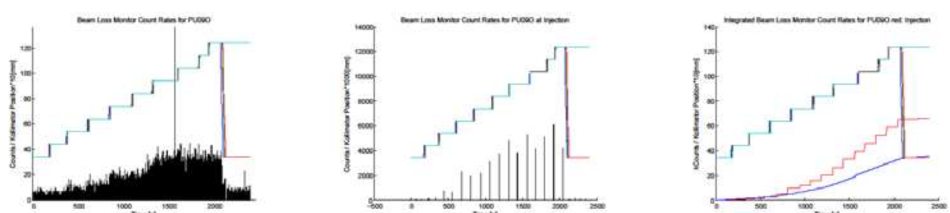

Figure 22: Count rates during stable beam operation (left), injection (center) and integrated over time for both (right) at 100mA in 960 bunches. The rates are somewhat lower (approximately a factor of 2) than those measured at PU02.

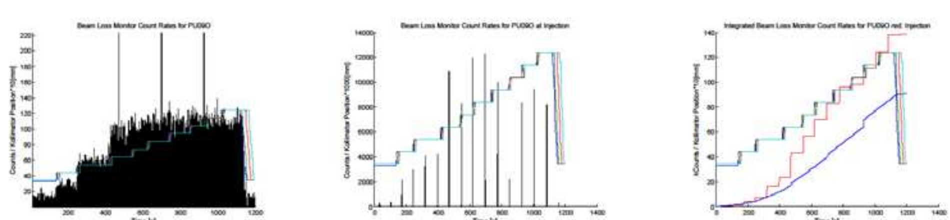

Figure 23: Count rates during stable beam operation (left), injection (center) and integrated over time for both (right) at 50mA in 40 bunches. The rates are somewhat lower (approximately a factor of 2) than those measured at PU02.

The count rates measured at PU09 are only slightly higher than those measured at PU02. A somewhat extraordinary feature of PU09 is that the cumulated rates of the injection exceed the ones for stable beam operation. That is likely to be an artefact of the way the measurement is executed. The injection losses are affected stronger by the collimator settings than the stable beam losses. The measurement integrates over quite some time with (almost) open collimators which leads to a distortion of the result.

2.4.4.6 First Tests with Cherenkov Fibers

Cherenkov fibers have been installed temporarily in sectors 1 and 2 along the undulators PU01a, PU01b, PU02 and PU03, and a series of test experiments have been performed. Figure 24 shows signals of a beam loss occurring during injection. The measurement has turn-by-turn resolution capabilities and provides additional amplitude information for the observed losses. However, the test experiments indicated that the measurement is not sensitive to stored beam loses, and only losses in the orbit plane could be observed. Nevertheless, an interesting result has been obtained from the measurements using the fiber. The signals appear typically with a frequency of 13 kHz which seems to correspond to the detuned horizontal tune for large amplitudes at injection. This indicates that the losses occur at large horizontal betatron amplitudes, where the vertical aperture is even more restricted due to the elliptic shape of the chambers.

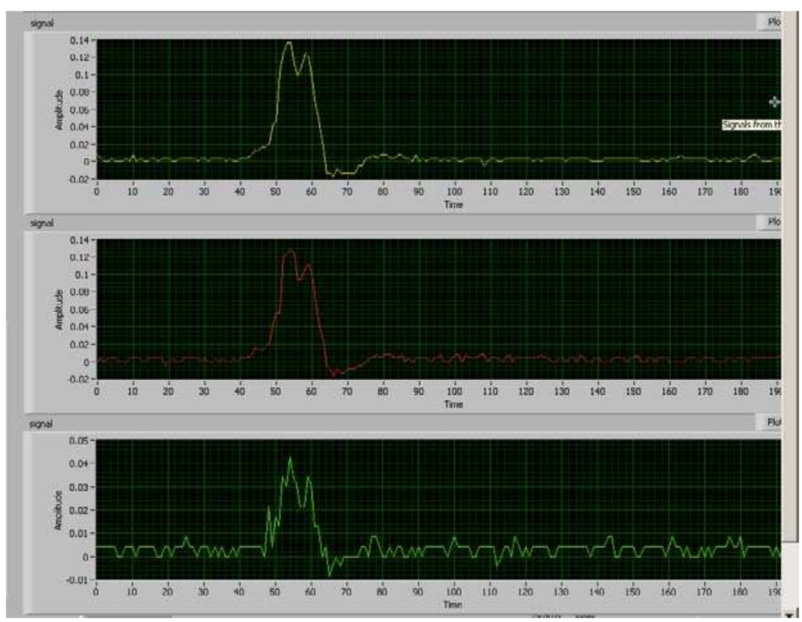

Figure 24: First signals of beam loss using the Cherenkov fiber installed in sector 1. Signal appearing in turn 1, 2 and 10.

Due to the insensitivity on the losses caused by the circulating beam which even could be observed with the PIN-photodiode based BLM system, in the future it is planned to increase the active detection volume and to test a Cherenkov based system which was originally designed for the European XFEL [19]. First test experiments which were performed at the ESRF look very promising.

2.4.5 Simulations Introduction

In the previous sections we have shown that radiation damage of insertion devices is observed in several places of the PETRA III undulator sections. It follows a general pattern that devices located at the entrance of a straight section are damaged at the upstream part while undulators installed at the exit of a straight section show signs of demagnetization at the downstream part. This seems to indicate that particle losses occur in the vertical plane at locations where the beta functions become large while the physical aperture limits are still very small. Whether these particle losses occur during injection; or are mainly caused by off-momentum particles remains to be clarified.

In order to gain more insight into the mechanism causing the radiation damage of the insertion devices, we embarked on a series of tracking studies using the tracking code SixTrack [10]. This code tracks particles through a magnetic lattice over large number of turns taking into account the full six-dimensional phase space including synchrotron oscillations in a simplistic manner. The systematic and random multipole measured field errors for each type of dipoles, quadrupoles, sextupoles, wigglers and correctors etc. are introduced to these magnets as thin nonlinear element at the center. The studies are performed for on energy as well as off-energy particles. Tracking studies were of course already performed during the design and commissioning phase of PETRA III [2, 11]. In those studies however, only the resulting dynamic and momentum aperture were recorded. No investigation on the loss patterns has been done. Actually, the presently used rather old version 1.1a of SixTrack does not generate separate output files for such a purpose. Therefore, we had to modify the code to get more direct access to the loss pattern.

The tracking studies are based on the standard PETRA III optics (p3_20wig) used during user operation containing the damping wigglers modeled in terms of a numerical generating function [12]. The model of the accelerator is put together by constructing a sequence of blocks of linear elements, nonlinear elements, observation points and possibly an RF cavity. The linear magnetic elements (dipoles, quadrupoles) are split into two linear parts and a thin nonlinear elements containing the multipole field errors. Consecutive linear elements are blocked together for fast tracking using a single transfer matrix. The particle trajectories are recorded at the 227 BPMs and several other particular longitudinal positions along the ring. The aperture limitations are introduced at several longitudinal positions in horizontal and vertical planes imposed by the physical aperture limitations of the vacuum system. For example, the absorbers in west (ABSW1-ABSW10)/north(ABSN1-ABSN10) damping wiggler section are elliptic in size with half apertures of 30 mm in the horizontal and 4.50/8.5 mm in the vertical plane. The undulator vacuum chambers have lower gaps than the absorbers in double bend achromat sections in the Max von Laue Hall. The beam position monitors (BPMs) in undulator sections have an elliptic vacuum chamber with half apertures of 30 mm in the horizontal and 5.25/3.5 mm in the vertical plane. Nonlinear elements such as sextupoles are modeled with half apertures of 40 mm in horizontal and 20 mm in the vertical plane. On top of that there is a general rectangular aperture check at each non-zero length elements. During tracking the particle is lost if the tracked orbit exceeds the physical aperture.

2.4.5.1 On Momentum Tracking

The on momentum tracking mainly aims at a better understanding of particle losses during injection. This is necessary to reduce the particle losses in the process of injection so that the radiation detectors (Pandoras) are at low rates to protect the activation at venerable locations. This also helps in finding the locations where the particles are lost due to unclosed kicker bumps. For the simulation particles are tracked with initial horizontal amplitudes increased from 0 mm to 55 mm in 111 steps. For every horizontal initial condition the vertical amplitude is varied in 81 steps starting from 0 mm using in step of 0.1 mm. The results of these tracking using 30 different error sets are shown in Figures 26(a, b). Depicted are the results for the tracking of 8991 on momentum particles. The color code is used to present the loss of particles for the aforesaid initial conditions tracked at 360 different block positions starting from South West of the ring. The two collimators (COLL1 in South West Right (SWR)), COLL2 in South West Left (SWL)) are open with half gaps of 40 mm, 20 mm. A maximum of 482 particles are lost out of 8991 near PU1a, b, which is 5.36%. The simulation shows that the losses are localized and independent of tracking starting block position and independent of random error sets, only the numbers of loss particles are changed. This means the loss of particles at local position PU01a is fixed for any random error sets or any start point of tracking, but only different number of particles lost are seen. As anticipated form the experiments during machine studies, the referred location of particle loss is at PU01a and PU01b. A comparable number of particles are lost in the damping wiggler section west at absorber ABSW9 (and/or damping wiggler section north at absorber ABSN9). It may be mentioned that the vertical aperture limitations are imposed first 4.5mm in west damping wiggler section followed by 4.5 mm in north damping wiggler section, 5.25 mm at PU01a,b and 3.5 mm at PU02 etc. The tracking shows that the particles are lost in vertical plane at those locations.

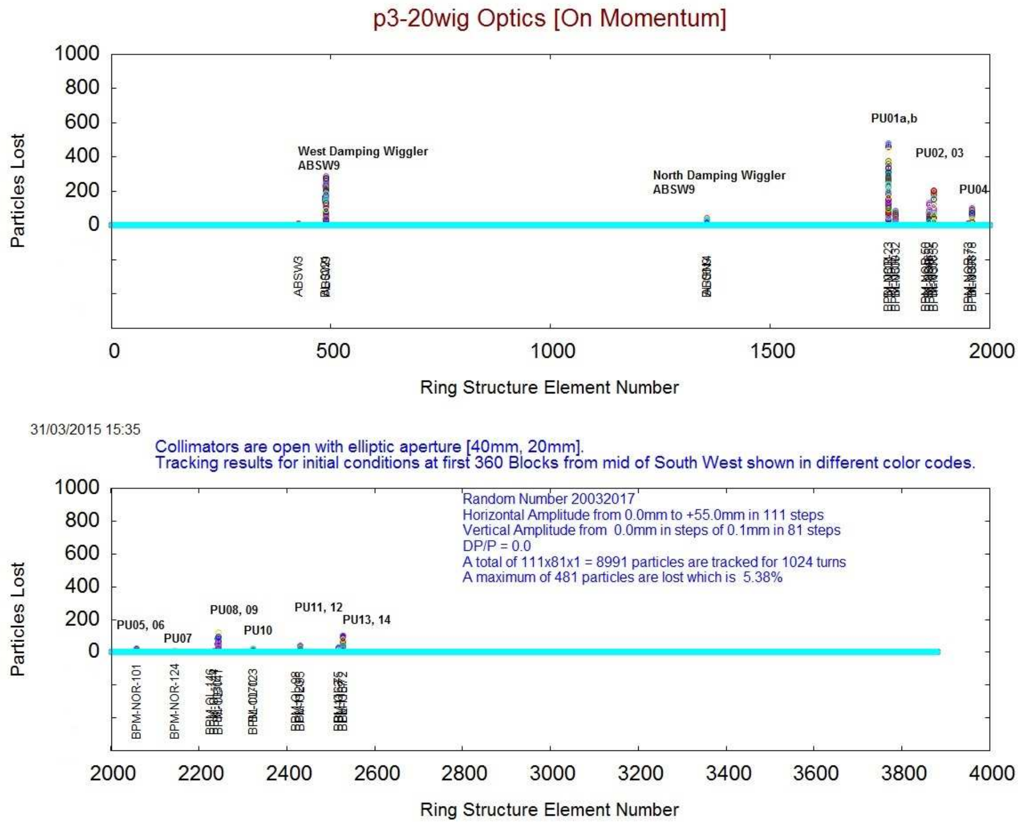

Figure 26a: Tracking results for on momentum particles with magnetic field errors tracked at 360 different structure element positions starting from South West for a single random number (Collimators are with elliptic aperture of 40mm, 20mm). A maximum of 482 particles are lost out of 8991 near PU1a, b, which is 5.36%.

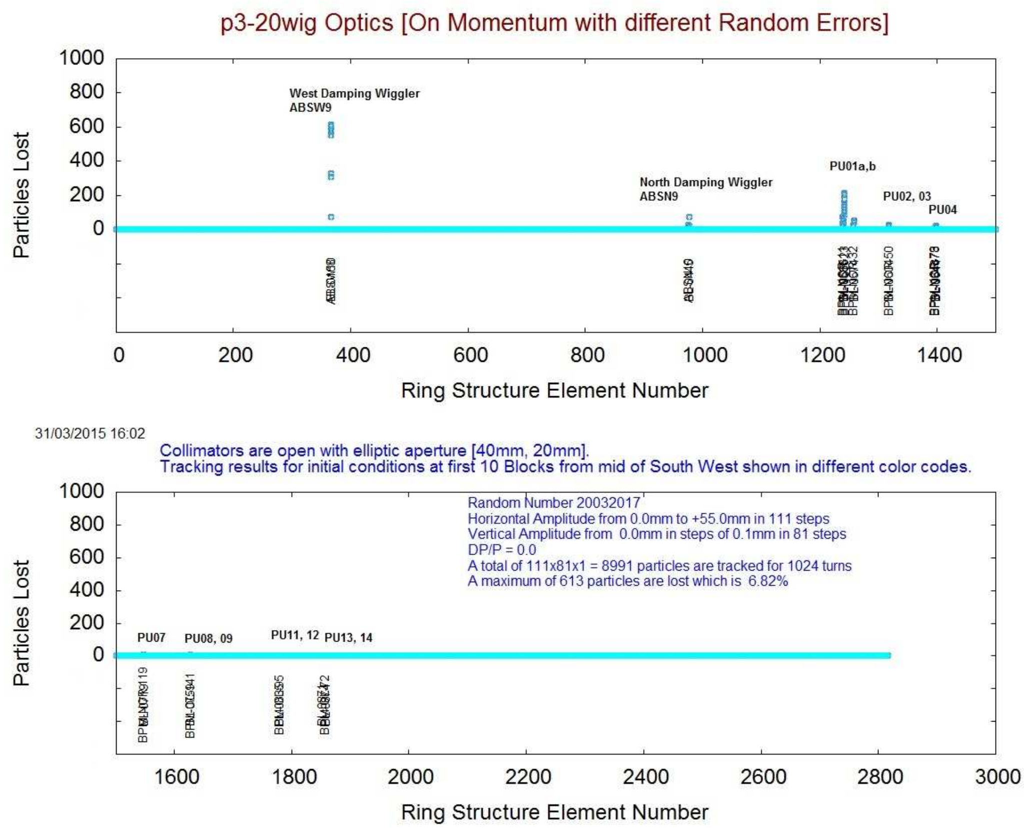

Figure 26b: Tracking results for on momentum particles with magnetic field errors tracked at 10 different structure element positions starting from South West for 30 random error sets (Collimators are with elliptic aperture of 40mm, 20mm). A maximum of 613 particles are lost out of 8991 near ABSW9, 10, which is 6.82%.

2.4.5.2 Off Momentum Tracking

In many third generation synchrotron light sources the beam lifetime is dominated by the Touschek effect [13, 14]. This is, in particular, also true for timing mode operation at PETRA III where typically 100 mA are stored in 40 evenly spaced bunches. The beam lifetime in this mode of operation is as low as 1.4 h. Typically, Top-Up leads to injections every 50 to 60 seconds when the beam current variation is limited to 1%. Since Touschek scattered particles suffer large longitudinal momentum deviations off momentum tracking studies were performed to gain insight into the local distribution of the lost particles.

Before we head for the details of the tracking simulation, one can ask the natural question whether the inspection of the off momentum optics of PETRA III indicates preferred locations of particle loss.

Using the MAD-X [15] code, where the chromatic functions are defined as

$$W_x = \sqrt{a_x^2 + b_x^2}, \qquad W_y = \sqrt{a_y^2 + b_y^2},$$

$$a_x = \frac{\partial \alpha_x}{\partial p_t} - \frac{\alpha_x}{\beta_x}\frac{\partial \beta_x}{\partial p_t}, \qquad a_y = \frac{\partial \alpha_y}{\partial p_t} - \frac{\alpha_y}{\beta_y}\frac{\partial \beta_y}{\partial p_t},$$

$$b_x = \frac{1}{\beta_x}\frac{\partial \beta_x}{\partial p_t}, \qquad b_y = \frac{1}{\beta_y}\frac{\partial \beta_y}{\partial p_t},$$

$$\phi_x = \frac{1}{2\pi}\tan^{-1}\left({a_x}/{b_x} \right), \qquad \phi_y = \frac{1}{2\pi}\tan^{-1}\left({a_y}/{b_y} \right),$$

one can look at the beta beating as a function of energy:

$$b_x = W_x Cos(2\pi\phi_x), \qquad b_y = W_y Cos(2\pi\phi_y),$$

$$a_x = W_x Sin(2\pi\phi_x), \qquad a_y = W_y Sin(2\pi\phi_y).$$

Since the apertures are small in the vertical plane, we try to analyze a_y at undulator sections for the standard optics (p3_20wig) of PETRA III. The optical functions together with the chromatic functions a_y and b_y are shown in Figure 25.

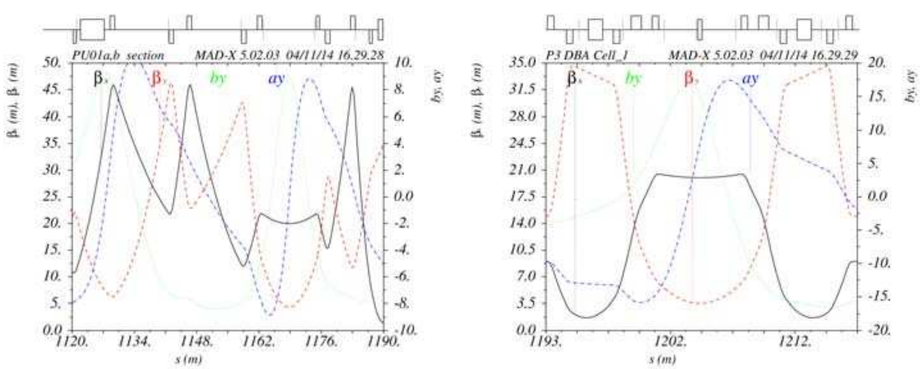

Figure 25: The computed values of a_y and b_y are plotted for the sections for undulator PU01 and PU02. The a_y value is high (negative) at the upstream of PU01 and PU02; as well as (positive) downstream of PU01 and PU02.

High losses are expected at extreme values of a_y. The major contribution of a_y comes from b_y, which is nothing else but the variation of beta with energy. The function a_y changes sign due to α_y. So, the loss of particles occur in vertical plane is due to variation of beta with energy. From these simple optics considerations it may be anticipated that off momentum particles are most likely lost at high a_y values. This matches with the BLMs measurements and is in accordance with the observed radiation damage. Collimators are foreseen in these sections to mitigate the sources of radiation damage.

Beyond linear optics considerations, a more precise treatment of particle losses due to large momentum offset caused by Touschek scattering would take into account the local nature of the physical process. The starting point would then be given by the local phase space distribution of Touschek scattered particles as generated by the stable beam. This takes into account that the scattering rate and distribution of particles depends on the local phase space density around the ring. Then this particle distribution could be tracked through the ring. Actually, the ring should rather be regarded as beamline in this context, because for a particle with considerable momentum deviation a closed solution might not exist. Touschek scattered particles might survive only a few turns or may even be lost within one turn. Recording the positions where the particles are lost provides the desired information about the beam loss pattern. It should be noted here that such an approach is adopted for the Elegant tracking code [16]. An even more complete picture might arise when one takes into account synchrotron radiation during tracking. A particle with energy excess after Touschek scattering might be recaptured when it radiates off some of its energy while travelling through a section with strong magnetic fields, as it is for instance the case in the damping wiggler section in PETRA III. The bottom line of this discussion is that the locally generated Touschek scattered particles might experience very different histories leading to deviations from the simple loss pattern predicted by scrutinizing the off energy optical functions. For PETRA III, however, this does not seem to be the case.

The approach adopted in the tracking studies here is simply to calculate local momentum apertures by tracking off momentum particles with various initial conditions and record their corresponding loss pattern. This obviously contains less quantitative information, because the mechanism how those particles are generated is ignored. A function, calculating distributions of Touschek scattered particles, is missing in SixTrack. Our main goal is to identify potential locations of cumulated particle loss. As it turns out this approach already provides a reasonable picture of the distribution of lost particles and is in good agreement with the considerations concerning the off momentum optical functions as presented above. The setup for the tracking studies is as follows.

The measured magnetic field errors are introduced to the magnets as thin elements. The particles are tracked with horizontal amplitude of -35 mm to 35 mm in 141 steps, vertical amplitude of 1 step from 0 mm instep of 0.1 mm. The momentum variations considered are $\Delta P/P$ from -0.02 to 0.02 in 41 steps. A total of 5781 particles are tracked with synchrotron oscillations for 8192 turns (damping times for 6.0GeV operation, τ_x = 84.66 ms, τ_y = 84.77 mm, τ_e = 42.41 ms with revolution time of T_0 = 7.68 μs) with magnetic field errors (with systematic and random), damping wigglers with errors at different initial positions for single random error set, where the collimators at SWL and SWR are open. The results of such tracking are shown in Figure 27. The results are shown in different colors for tracking at 384 different initial block positions starting from South West of the ring. A maximum of 606 particles are lost out of 5781 near PU1a, b, which is 10.48%. Similar to the on momentum tracking, here the simulation shows also that the losses are localized at certain positions and are independent of tracking starting block position and are independent of random error sets, only the numbers of loss particles are changing. This means the loss of particles at local position PU01a is fixed for any random error sets or any start point of tracking, but only different number of particles lost are seen. The obvious point of high loss is at PU01a, b which is experimentally seen. Similar is the case for damping wiggler section where most of the particles are lost. It is quite noticeable from Figure 27 that a comparable number of particles are lost at sextupoles locations. The severe losses are observed at longitudinal position of S2_NR_118. We have no monitoring system at this location. We have seen radiation damage at up and downstream locations of PU02 which is reproduced in tracking results. The tracking results shows severity at PU04 as mentioned in integrated TLD dose rate, unfortunately we do not have field measurement data for PU04.

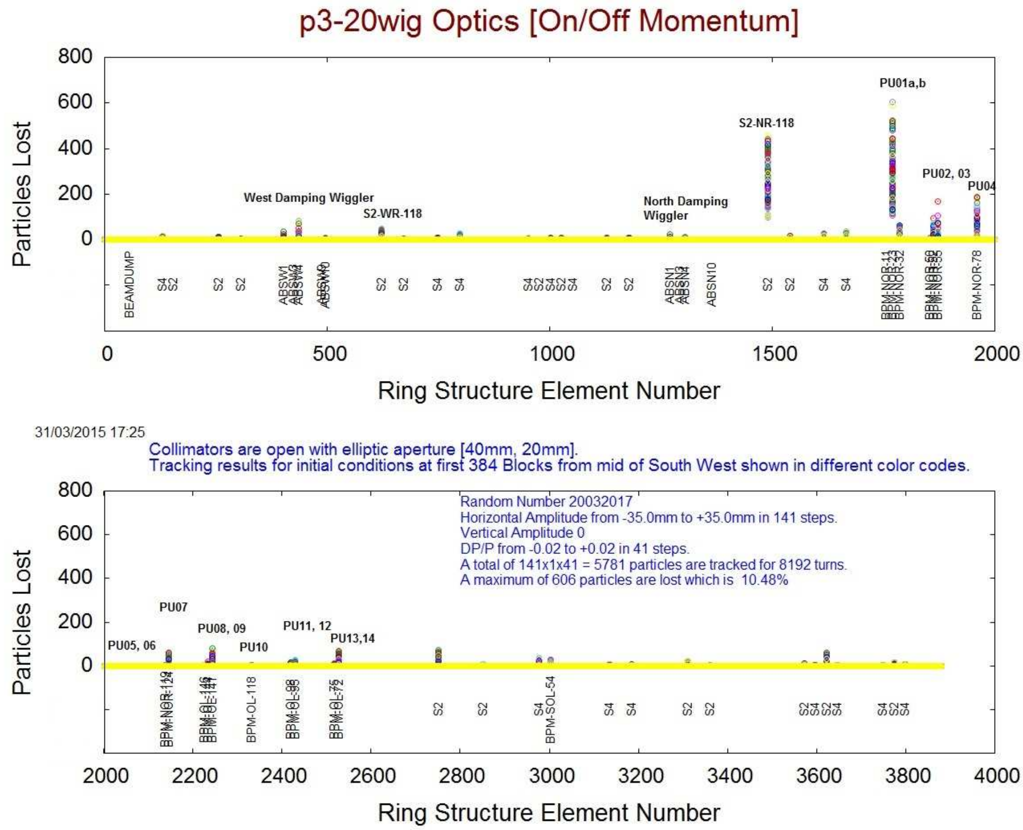

Figure 27: Tracking results for off momentum (ΔP/P = -0.02 to 0.02) particles with magnetic field errors tracked at 384 different structure element positions starting from South West for a single random number (Collimators are open). A maximum of 606 particles are lost out of 5781 near PU1a, b, which is 10.48%.

Now, it is time to vary the collimator settings to observe the influence on beam losses at different positions. We have observed during earlier experiments that the BLMs show less count rates with collimator settings closed to some minimum positions (say ±4 mm). This suggests that the particles are lost somewhere else! In the following Figures 28(a,b,c) the tracking results with off momentum particles are shown for different closing positions of collimators at COLL2 and COLL1. If the vertical closing apertures becomes smaller and smaller (6 mm to 3.5 mm) the loss of particles increases at the collimators from 12.35% to 24.72% which explains effective scrapping by the collimators. The loss rate is drastically reduced at all undulator locations except PU04 which is blind to these collimators. Still appreciable loss is observed at S2_NR_118 even with closed collimators. The radiation doses measured in the inner side of the ring on 22.01.2014 in the PETRA III tunnel are produced herewith (Table 1) from the PETRA eLogbook for comparison with the tracking results. It may be noted that tracking shows heavy loss at S2_NR_118 which is clearly seen in the measured data. Figure 28d shows that the losses of particles are at S2_WR_118, S2_NR_118, S2_SOR_83 is also in the inner side.

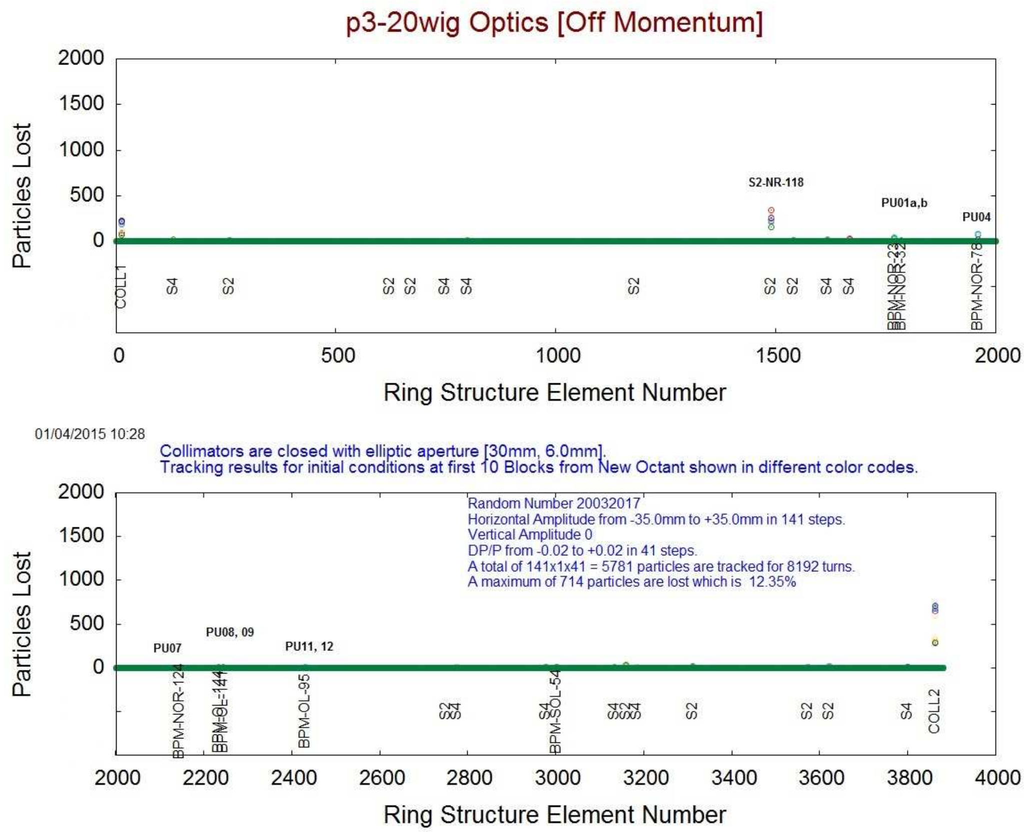

Figure 28a: Tracking results for off momentum ($\Delta P/P$ = -0.02 to 0.02) particles with magnetic field errors tracked at 20 different longitudinal positions starting from New Octant for a single random number (Collimators are closed at 6.0 mm, maximum of 714 particle lost at COLL2 which is 12.35%).

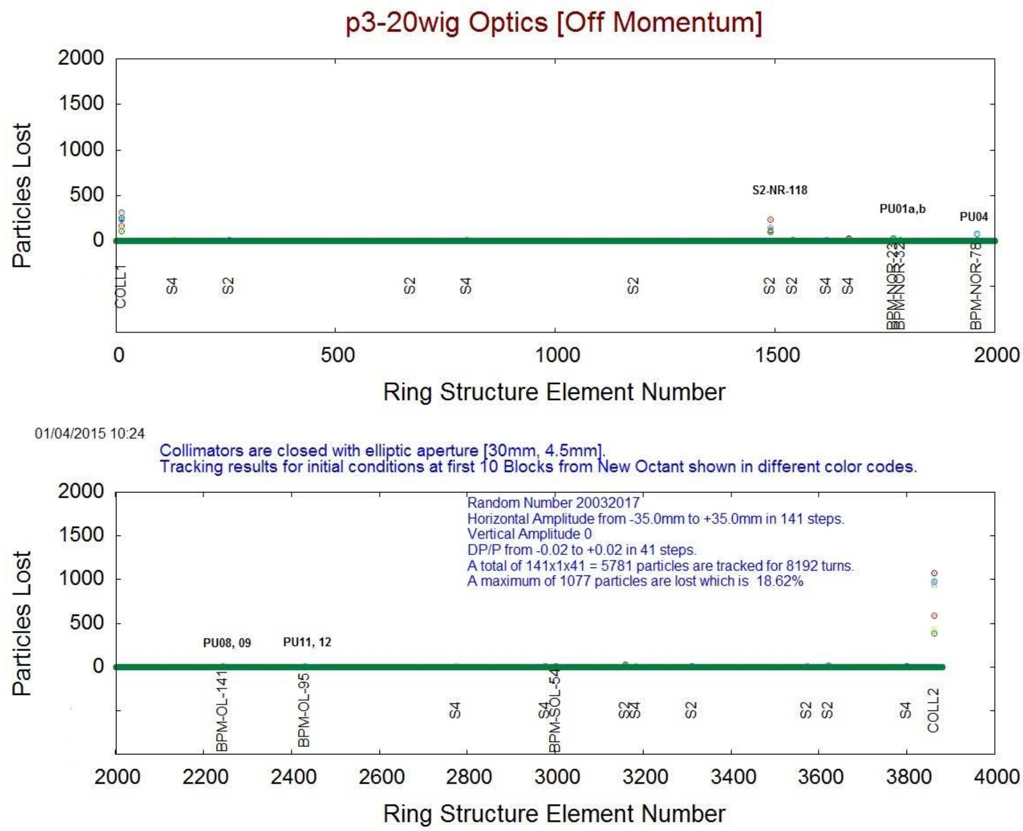

Figure 28b: Tracking results for off momentum ($\Delta P/P$ = -0.02 to 0.02) particles with magnetic field errors tracked at 20 different longitudinal positions starting from New Octant for a single random number (Collimators are closed at 4.5 mm, maximum of 1077 particle lost at COLL2 which is 18.62%).

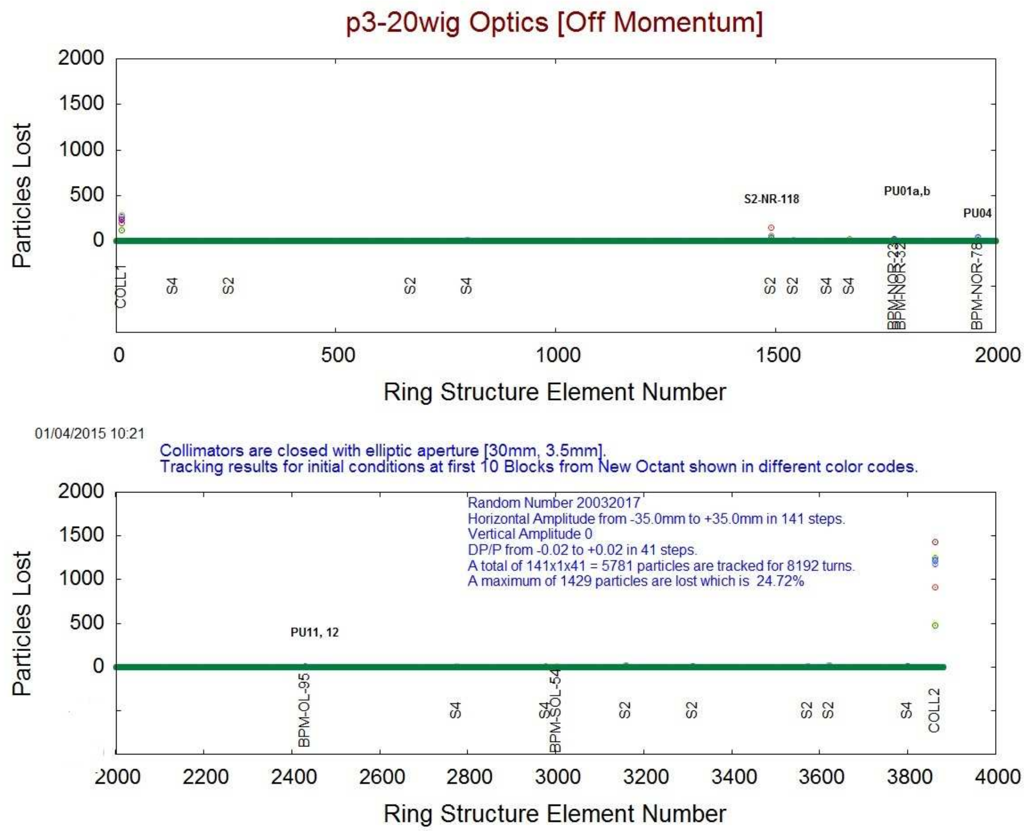

Figure 28c: Tracking results for off momentum ($\Delta P/P$ = -0.02 to 0.02) particles with magnetic field errors tracked at 20 different structure element positions starting from New Octant for a single random number (Collimators are closed at 3.5 mm, maximum of 1429 particle lost at COLL2 which is 24.72%).

Table 1: Logbook entry on 22.01.2014 which is reproduced here along with tracking results.

Location	**Rate [µSv]**	Particles Lost
NR_118	100	456
WR_118	17	49
NWR_83	20	2
OR_118	9	
SOR_83	80	38

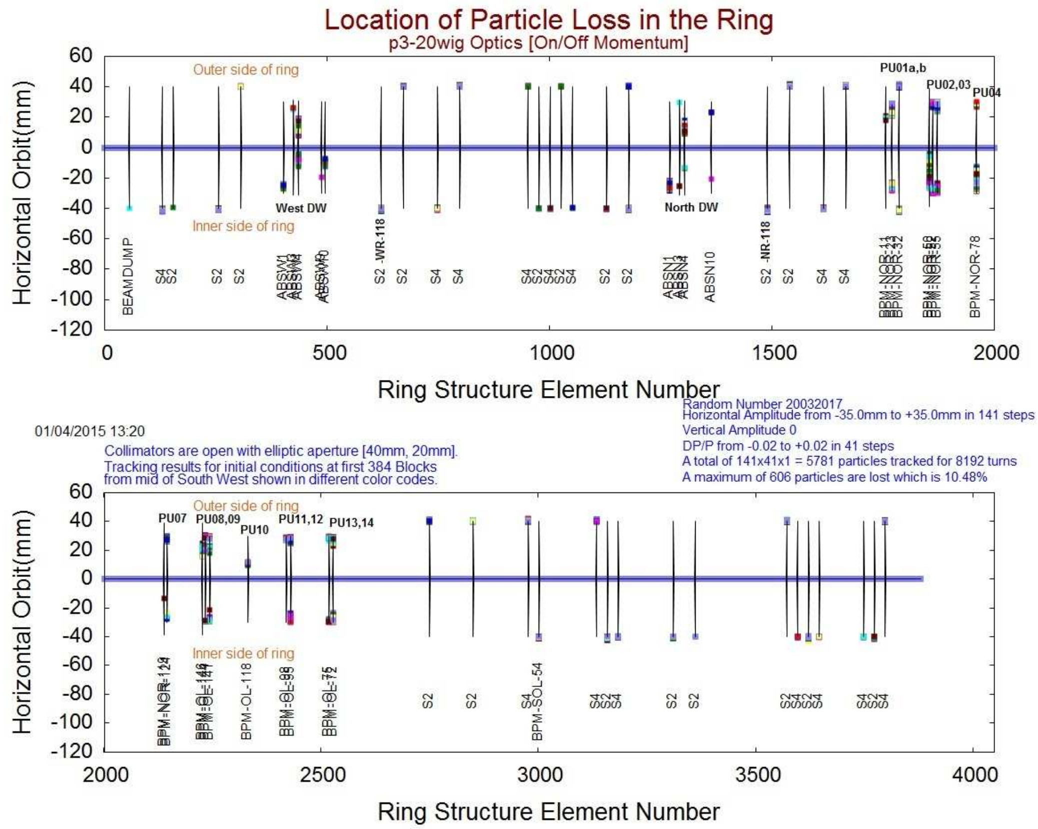

Figure 28d: Tracking results for off momentum (ΔP/P = -0.02 to 0.02) particles with magnetic field errors tracked at 384 different longitudinal positions starting from south west for a single random number (Collimators are open). Here the end horizontal orbits are shown at loss points to indicate in/out side of the ring. The solid lines indicate the available physical apertures.

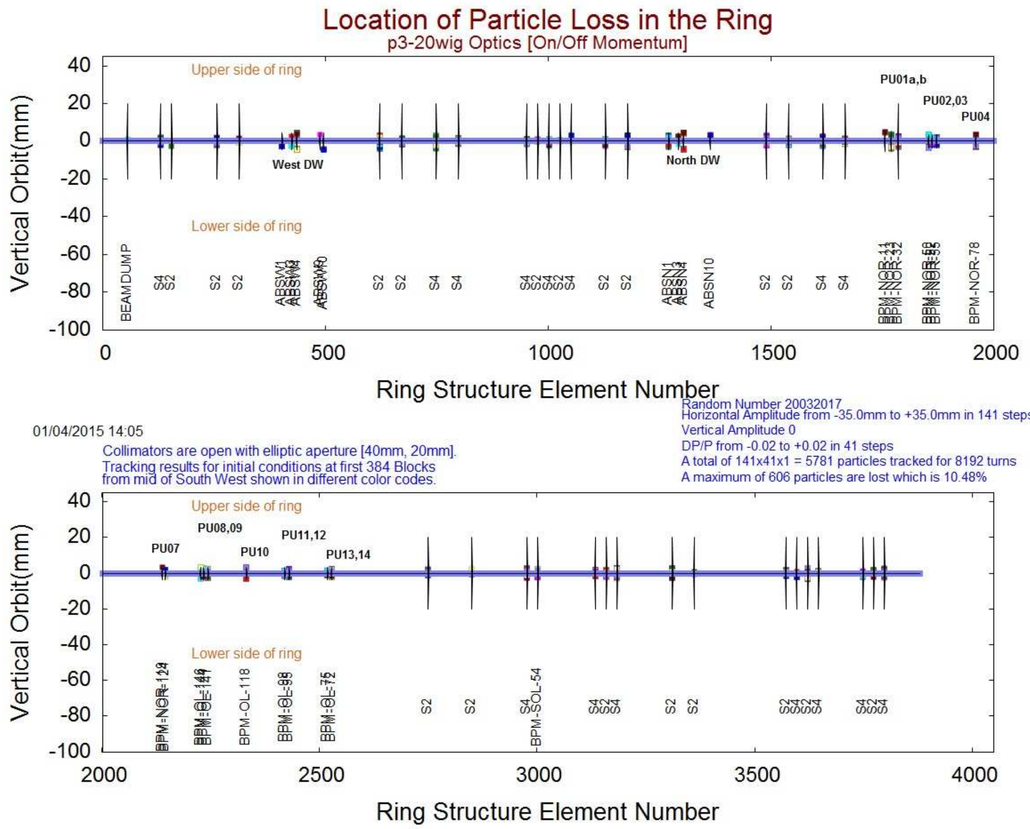

Figure 28e: Tracking results for off momentum (ΔP/P = -0.02 to 0.02) 5781 particles with magnetic field errors tracked at 384 different longitudinal positions starting from south west for a single random number (Collimators are open). Here the end vertical orbits are shown at loss points to indicate up/down side of the ring. The solid lines indicate the available physical apertures.

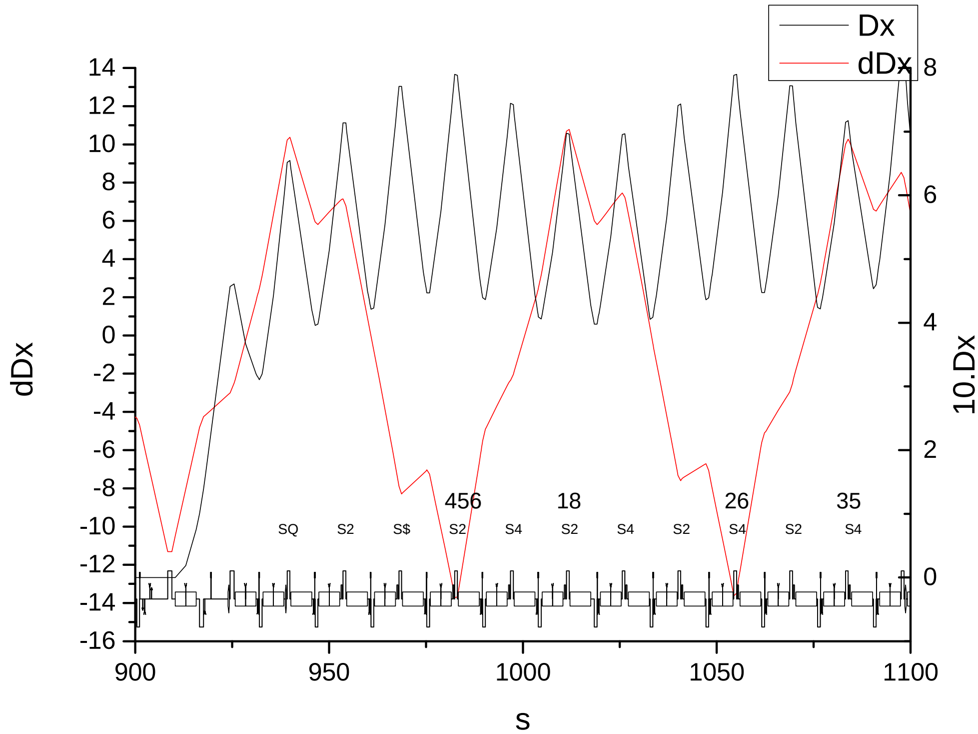

Figure 29: The horizontal dispersion function D_x magnified by a factor of 10 and its chromatic derivative dD_x plotted in the achromat section just after the north damping wiggler section for p3_20wig optics of PETRA III as computed by MAD-X. The particle losses from tracking simulations with SixTrack are shown along with the sextupole names.

In this achromat section some correlation is seen between the loss of particles in the tracking and the measured data in the PETRA tunnel that we have already mentioned above. But, as shown in the Figure 29, the losses are at high dispersion and its high chromatic derivative of D_x locations. For positive chromatic derivative D_x the loss is outside of the ring and for negative chromatic derivative D_x the loss is inner side of the ring. The radiation activation at S2_NR_118 which was measured in the inner side of the tunnel is corresponding to negative dDx. At other sextupole locations S2, S4 and S4 the radiation activation is outside, inside and outside of the ring corresponding to positive or negative of dD_x. The loss of particles at S2_WR_118 and S2_SOR_83 is also at the inner side which is explained in a similar way.

2.4.6 Conclusions

Radiation damage of insertion devices is observed in several places of the PETRA III undulators. It follows a general pattern that devices located at the entrance of a straight section are damaged at the upstream end while undulators installed at the exit of a straight sections show signs of demagnetization at the downstream end. This seems to indicate that particle losses occur in the vertical plane at locations where the beta functions become large while the physical aperture limits are still very small. The tracking results showed the losses at the beam line positions where severe demagnetization had occurred confirming that this might have avoided by proper collimation. The optics studies shows major contribution to the losses at the location of high a_y resulting from high b_y, which is nothing but higher beta beating with energy at very low physical aperture. So, one could say that the large beta beat for particles with energy deviation at the limiting vertical apertures in these straight sections are consistent with primarily off-momentum particle loss in those regions, supported by the measured indication of losses in those areas as Touschek scattered particles suffer large longitudinal momentum deviations. For a better protection the IDs against radiation damage additional collimators at high β_y values have been recently installed in April 2015.

2.4.7 Acknowledgements

The authors gratefully acknowledge and would like to thank Nicholas John Walker for reading the manuscript, suggestions to improve the content of the paper and constant encouragements and guidance. The authors also acknowledge and thank colleagues involved in measurements from FS-PE and M-Division for their fruitful contributions.

2.4.8 References

1. K. Balewski, W. Brefeld, et al., “PETRA III: A new high brilliance synchrotron radiation source at DESY”, EPAC-2004, Lucerne, 2004, pp.2302-2304.
2. K. Balewski et al., “PETRA III, A low emittance Synchrotron Radiation Source”, Technical Design Report, DESY 2004-035.
3. K. Balewski, M Bieler, et al., “PETRA III Upgrade”, Proceedings of 2nd International Particle Accelerator Conference (IPAC11), San Sebastian, Spain, 4-9, September 2011, pp. 2948-2950.
4. N. Simos**,** P. K. Job, et al., “An experimental study of radiation-induced demagnetization of insertion device permanent magnets”, BNL-81453-2008-CP, 2008.
5. J. Chavanne, P. Elleaume, et al., “Partial demagnetization of ID6 and dose measurements on certain IDs”, ESRF Machine Technical Note 1-1996/ID, 1996.
6. E.R. Moog, P.K. DenHartog, et al., “Radiation doses to insertion devices at the advanced photon source”, The 10th United States national conference on synchrotron radiation instrumentation. AIP Conference Proceedings, Volume 417, pp. 219-223 (1997).
7. P. Vagin, O. Bilani, et al., “Radiation Damage of Undulators at PETRA III”, Proceedings of IPAC2014, Dresden, Germany, 2014.
8. P. Vagin, S. Francoual, J. Keil, O. H. Seeck, J. Strempfer, A. Schöps, M. Tischer “Commissioning Experience with Undulators at PETRA III”, Proceeding of SRI2012, Lyon, July 2012, http://iopscience.iop.org/1742-6596/425/3
9. M. Tischer, P. Vagin, “Demagnetization Effects PETRA III Undulators”, this Beam Dynamics Newsletter
10. F. Schmidt, “SixTrack User’s Reference Manual”, CERN/SL/94-56 (AP), CERN, Geneva, 2012.
11. A. Kling, R. Wanzenberg , “Beam Dynamics Activities at PETRA III”, Published in ICFA Beam Dyn.Newslett.62, pp. 235-243, 2013.
12. W. Decking, O. Kaul, et al.,”Treatment of wiggler and undulator field errors in tracking codes”, IEEE PAC 1995, pp. 2874-2876.
13. A. Piwinski, “The Touschek Effect in Strong Focusing Storage Rings”, DESY 98-179. 1998.
14. F. Wang, “Touschek Lifetime Calculations for the NSLS-II Electron Storage Ring”, MIT-Bates Linear Accelerator Center, Middleton , MA 01949, 2006.

15. H. Grote, F. Schmidt, et al., “The MAD-X Program (User's Reference Manual)”, CERN, Geneva, 2015.
16. M. Borland, “elegant: A Flexible SDDS-compliant Code forAccelerator Simulation”, APS LS-287, September 2000.
17. K. Wittenburg, “The PIN-Diode Beam Loss Monitor System at HERA“, Proc. BIW2000, Cambridge, MA (2000).
18. W. Goettmann et al., "Beam Loss Position Monitor using Cerenkov Radiation in Optical Fibers", Proc. DIPAC 2005, Lyon, France (2005), POW026.
19. A. Kaukher et al., „XFEL Beam Loss Monitor Sytem“, Proc. BIW2012, Newport News, VA (2012) MOPG007.
20. A. Klett, A. Leuschner, „A Pulsed Neutron Monitor“, IEEE 2007 Nuclear Science Symposium, Conf. Records, Oct. 27 -Nov 3, 2007, Honolulu, Hawaii, US

3 Workshop and Conference Reports

3.1 ICFA Advanced Beam Dynamics Workshop “AOC2015” enables accelerator experts to meet optics challenges of future machines

M. Giovannozzi, R. Tomás, F. Zimmermann, CERN
Mail to: Massimo.Giovannozzi@cern.ch

About 50 experts attended the ICFA beam dynamics workshop on Advanced Optics Control (AOC) hosted at CERN in February 2015 (Thursday 5th and Friday 6th), in order to discuss the frontiers and future directions of accelerator optics control for colliders, light sources, and other specialized storage rings. The details of the program as well as a collection of all talks are available on the indico web site http://indico.cern.ch/event/349643

In addition to ICFA, the AOC workshop was also sponsored and supported by EuCARD-2 XBEAM, EuCARD-2 XRING, HIC for FAIR, ICFA, CERN PS MTE, HiLumi LHC, LIU, and CERN. The large number of sponsoring organizations reflects the importance of the topics addressed and their relevance for many future projects.

AOC2015 was the third workshop devoted to optics measurements, corrections, and control, following two earlier workshops organized in the frame of EuCARD-AccNet, i.e. the 2011 EuCARD-AccNet workshop on Optics Measurements, Corrections and Modeling for for High-Performance Storage Rings (http://indico.cern.ch/event/132526) and the LHC Optics Measurement and Corrections review (http://indico.cern.ch/event/246159) in 2013.

One key topic of AOC2015 was the lessons from LHC Run-1 and the preparation for the LHC Run-2. Interesting new diagnostics and modelling approaches were reported from various state-of-the-art light sources. Optics challenges for future machines were also reviewed, including the High-Luminosity LHC, the Future Circular Colliders for hadron and leptons, new light sources like the ESRF upgrade, special storage rings dedicated to measuring the electric dipole moment of protons or deuterons.